

Article

## Tuning NaYF<sub>4</sub> Nanoparticles through Alkaline Earth Doping

Xian Chen <sup>1</sup>, Dengfeng Peng <sup>1</sup> and Feng Wang <sup>1,2,\*</sup>

<sup>1</sup> Department of Physics and Materials Science, City University of Hong Kong, 83 Tat Chee Avenue, Hong Kong; E-Mails: zjuchenxian@gmail.com (X.C.); dengpeng@cityu.edu.hk (D.P.)

<sup>2</sup> City University of Hong Kong Shenzhen Research Institute, Shenzhen 518057, China

\* Author to whom correspondence should be addressed; E-Mail: fwang24@cityu.edu.hk; Tel.: +852-3442-4898; Fax: +852-3442-0538.

Received: 10 October 2013; in revised form: 20 October 2013 / Accepted: 21 October 2013 /

Published: 24 October 2013

---

**Abstract:** Phase and size of lanthanide-doped nanoparticles are the most important characteristics that dictate optical properties of these nanoparticles and affect their technological applications. Herein, we present a systematic study to examine the effect of alkaline earth doping on the formation of NaYF<sub>4</sub> upconversion nanoparticles. We show that alkaline earth doping has a dual function of tuning particle size of hexagonal phase NaYF<sub>4</sub> nanoparticles and stabilizing cubic phase NaYF<sub>4</sub> nanoparticles depending on composition and concentration of the dopant ions. The study described here represents a facile and general strategy to tuning the properties of NaYF<sub>4</sub> upconversion nanoparticles.

**Keywords:** impurity doping; nanoparticles; phase transformation; upconversion

---

### 1. Introduction

The synthesis of lanthanide-doped upconversion (UC) nanoparticles with well-defined phase and size is important for understanding the enormously complex optical transitions in the host lattice [1–3] and for realizing applications of these nanoparticles in solid-state lasers, three-dimensional flat-panel display, solar cells and especially biolabeling and bioimaging [4–15]. The phase and size of lanthanide-doped nanoparticles are usually tuned by controlling the thermodynamic or kinetic growth of the nanoparticles through manipulation of several experimental variables, such as temperature, reaction time, and relative concentrations of the precursors [16–20]. The major problems of these approaches includes the difficulty in fine tune the nanoparticle size over a broad range and the need for extreme reaction conditions such as toxic reactants and high temperatures [21–23].

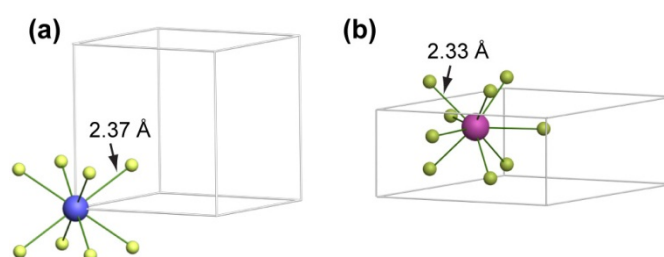
Impurity doping that involves incorporating suitable foreign ions into a host lattice has recently emerged as a promising alternative to control the formation of lanthanide-doped nanoparticles [24–29]. The doping approach usually allows the fine tuning of a variety of nanoparticle properties including phase, size, and even shape following a facile and standard synthetic procedure by simple modification of dopant composition and concentration [24–34]. Doping also modifies free energies of a materials system and stabilizes a particular crystal phase or particle morphology that is typically inaccessible by a common synthetic method [35,36].

For better understanding and control of doping-mediated crystal growth process, herein we describe the synthesis and characterization of a series of NaYF<sub>4</sub>:Yb/Er nanoparticles in the presence of alkaline earth dopant ions of varying composition (Sr<sup>2+</sup> and Ca<sup>2+</sup>) and concentration (0–60 mol %). As one of the most studied upconversion materials, NaYF<sub>4</sub> nanoparticles generally crystallize in either the cubic or hexagonal form. We show that the Sr<sup>2+</sup> or Ca<sup>2+</sup> dopant ions can significantly modify the phase and size of the as-synthesized NaYF<sub>4</sub>:Yb/Er nanoparticles through precise control of dopant concentration. We also correlate upconversion emission of the nanoparticles with the dopant composition and concentration by optical measurement.

## 2. Results and Discussion

Previous investigations suggest that in wet chemical synthesis NaYF<sub>4</sub> nanoparticles usually crystallize in cubic phase at first, which spontaneously transformed to the corresponding hexagonal phase as the reaction proceeds [16,37]. The cubic to hexagonal phase transformation of NaYF<sub>4</sub> is accompanied by a distortion and compression in electron cloud of the cation ions to accommodate the more asymmetric and dense hexagonal crystal structure (Figure 1). We reasoned that the presence of impurities of significant larger ionic size than Y<sup>3+</sup> ( $r = 1.159 \text{ \AA}$ ) [38] in the host lattice should suppress the phase transformation by increasing the energy barrier, thereby stabilizing the cubic phase product.

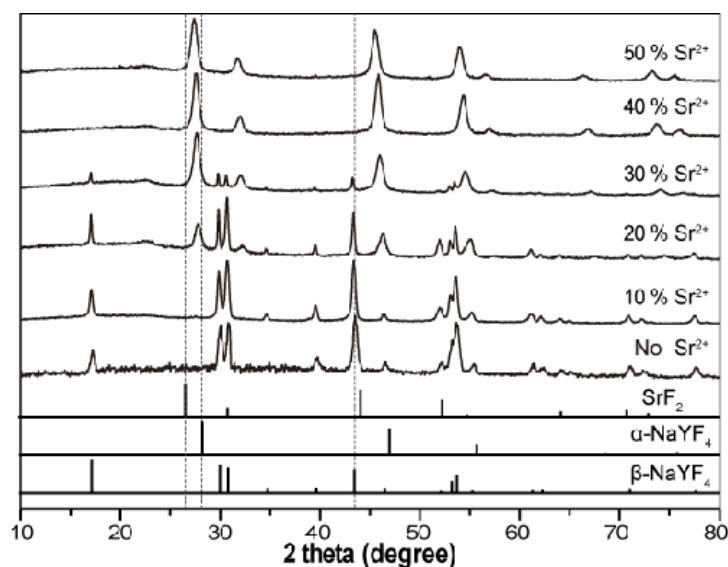
**Figure 1.** A comparison of the crystal site for the metal ions in the (a) cubic and (b) hexagonal phase NaYF<sub>4</sub>.



As a proof-of-concept experiment, Sr<sup>2+</sup> ions ( $r = 1.40 \text{ \AA}$ ) [38] that are optically inactive and chemically compatible with trivalent lanthanide ions were introduced to modify the growth process of NaYF<sub>4</sub>:Yb/Er nanoparticles. A series of samples obtained in the presence of Sr<sup>2+</sup> ions at different concentrations (0–50 mol %) were first examined by X-ray diffraction (XRD). As shown in Figure 2, XRD pattern of the Sr<sup>2+</sup> free sample can be indexed as pure hexagonal phase NaYF<sub>4</sub> (JCPDS file number 16-0334 [39]), which is consistent with previous studies [16,24]. On doping with increased Sr<sup>2+</sup> concentrations, the preservation of the cubic phase in these samples is evident and pure cubic

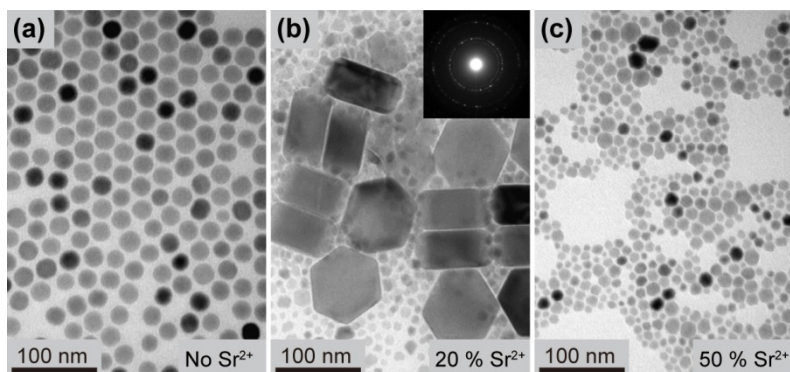
phase NaYF<sub>4</sub>:Yb/Er nanoparticles was obtained when the Sr<sup>2+</sup> ion concentration reached 40 mol %. The observed single cubic phase at a significantly high Sr<sup>2+</sup> dopant concentration (50 mol %) can be attributed to the small structural difference between the cubic phase NaYF<sub>4</sub> and SrF<sub>2</sub>. Notably, the diffraction peaks shift towards low diffraction angles with increasing dopant concentration of Sr<sup>2+</sup>, which results from expansion in unit-cell volume due to the larger Sr<sup>2+</sup> dopant ions and confirms the formation of a homogeneous Y-Sr solid solution.

**Figure 2.** X-ray diffraction (XRD) patterns of the NaYF<sub>4</sub>:Yb/Er (18/2 mol %) nanoparticles obtained in the presence of different amount of Sr<sup>2+</sup> dopant ions. The bottom line spectra are literature data for cubic phase SrF<sub>2</sub> (JCPDS file number 06-0262 [40]), cubic phase NaYF<sub>4</sub> (JCPDS file number 77-2042 [41]) and hexagonal phase NaYF<sub>4</sub> (JCPDS file number 16-0334 [39]), respectively.



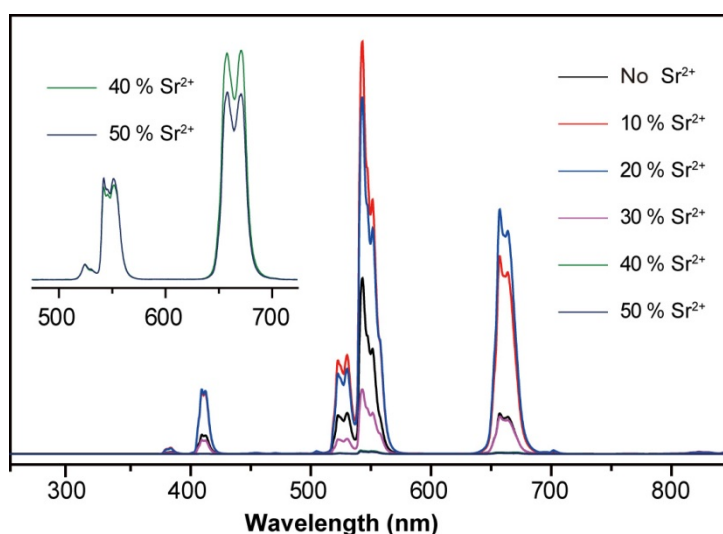
Transmission electron microscopy (TEM) characterizations were then carried out to study the morphology and size of NaYF<sub>4</sub>:Yb/Er (18/2 mol%) samples doped with Sr<sup>2+</sup> ions at different concentrations. Figure 3a presents the Transmission electron microscopy (TEM) image of the NaYF<sub>4</sub>:Yb/Er nanoparticles without Sr<sup>2+</sup> doping and shows uniform nanoparticles with a spherical morphology. In the presence of Sr<sup>2+</sup> (20 mol %), the TEM images shows two distinct particle morphologies including small irregular particles and large hexagon prisms (Figure 3b), which is consistent with the presence of two phases observed by XRD. Selected area electron diffraction analysis reveals that the small nanoparticles are cubic phase NaYF<sub>4</sub> (Figure 3b, inset). We therefore concluded the large prisms to be hexagonal phase NaYF<sub>4</sub>. The increase in particle size of the hexagonal phase product is attributed to the increased positive charge density associated with substitutional Sr<sup>2+</sup> ions at the nanoparticle surface, which promote the nanoparticle growth and results in a larger particle size [42]. With increasing dopant concentration of Sr<sup>2+</sup> (50 mol %), the large prisms disappeared (Figure 3c), suggesting the formation of pure cubic phase NaYF<sub>4</sub> nanoparticles.

**Figure 3.** Transmission electron microscopy (TEM) images of the NaYF<sub>4</sub>:Yb/Er (18/2 mol %) nanoparticles obtained in the presence of (a) 0 mol %, (b) 20 mol %, and (c) 50 mol % of Sr<sup>2+</sup> dopant ions, respectively.



We next investigated optical properties of the NaYF<sub>4</sub>:Yb/Er nanoparticles as a function of Sr<sup>2+</sup> dopant concentration. Figure 4 depicts the upconversion emission spectra of the nanoparticles doped with varying amount of Sr<sup>2+</sup> ion under 976-nm diode laser excitation. Characteristic emission peaks at 409 nm (blue), 526 and 545 nm (green), and 660 nm (red) were observed and assigned to <sup>2</sup>H<sub>9/2</sub>→<sup>4</sup>I<sub>15/2</sub>, <sup>2</sup>H<sub>11/2</sub>, <sup>4</sup>S<sub>3/2</sub>→<sup>4</sup>I<sub>15/2</sub>, and <sup>4</sup>F<sub>9/2</sub>→<sup>4</sup>I<sub>15/2</sub> transitions of Er<sup>3+</sup>, respectively. The spectra shows that the emission intensity is slightly enhanced at low Sr<sup>2+</sup> content (<20 mol %), which is attributed to the formation of large hexagonal prism. Further increase in Sr<sup>2+</sup> dopant concentration results in a sharp decrease in the emission intensity because of the phase transformation from hexagonal to cubic. The amplified spectra (inset) reveal that the red-to-green intensity ratio is largely increased at high Sr<sup>2+</sup> content, which is partly due to the formation of small sized cubic phase nanoparticles.

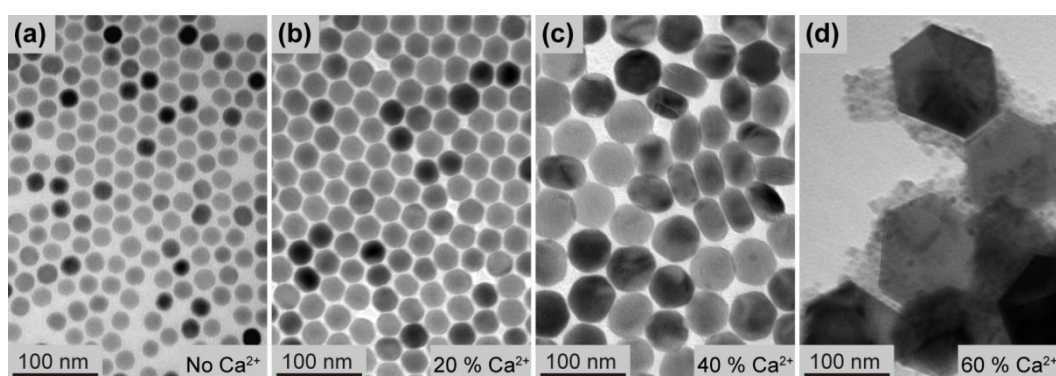
**Figure 4.** Upconversion emission spectra of the NaYF<sub>4</sub>:Yb/Er (18/2 mol %) nanoparticles obtained in the presence of different amount of Sr<sup>2+</sup> dopant ions. Inset: amplified spectra of the nanoparticles comprising high dopant concentration of Sr<sup>2+</sup>.



In a further set of experiments, we examined the effect Ca<sup>2+</sup> doping on crystal growth process of the NaYF<sub>4</sub>:Yb/Er nanoparticles. TEM images (Figure 5) of the as-synthesized nanoparticles all show no

phase separation for dopant concentrations below 40 mol %, suggesting that the cubic phase was not effectively stabilized by  $\text{Ca}^{2+}$  ions. The observation can be ascribed to the smaller ionic size of  $\text{Ca}^{2+}$  ions ( $r = 1.26 \text{ \AA}$ ) [38] than that of  $\text{Sr}^{2+}$  and therefore the relatively high amenability to the phase transformation into the dense hexagonal structure. Nevertheless, the nanoparticle size is fine-tuned through precise control of the  $\text{Ca}^{2+}$  dopant concentration. The steady increase in the nanoparticle size with increasing  $\text{Ca}^{2+}$  dopant concentration is mainly due to surface charge modification similar as for the Sr-doped samples.

**Figure 5.** TEM images of the  $\text{NaYF}_4:\text{Yb}/\text{Er}$  (18/2 mol %) nanoparticles obtained in the presence of (a) 0 mol %, (b) 20 mol %, (c) 40 mol %, and (d) 60 mol % of  $\text{Ca}^{2+}$  dopant ions, respectively.



### 3. Experimental Section

$\text{Y}(\text{CH}_3\text{COOH})_3 \cdot x\text{H}_2\text{O}$  (99.9%),  $\text{Yb}(\text{CH}_3\text{COOH})_3 \cdot x\text{H}_2\text{O}$  (99.9%),  $\text{Er}(\text{CH}_3\text{COOH})_3 \cdot x\text{H}_2\text{O}$  (99.9%),  $\text{Sr}(\text{CH}_3\text{COOH})_2 \cdot 2\text{H}_2\text{O}$ ,  $\text{Ca}(\text{CH}_3\text{COOH})_2$  ( $\geq 99\%$ ),  $\text{NaOH}$  ( $>98\%$ ),  $\text{NH}_4\text{F}$  ( $>98\%$ ), 1-octadecene (90%), oleic acid (90%), were all purchased from Sigma-Aldrich and used as starting materials without further purification.

In a typical procedure for the synthesis of  $\text{NaYF}_4:\text{Yb}/\text{Er}$  nanoparticles, 2 mL aqueous solution (0.2 M) of  $\text{RE}(\text{CH}_3\text{COOH})_3$  ( $\text{RE} = \text{Y}$ ,  $\text{Yb}$  and  $\text{Er}$ ) and  $\text{AE}(\text{CH}_3\text{COOH})_2$  ( $\text{AE} = \text{Sr}$  and  $\text{Ca}$ ) was added to a 50 mL flask containing oleic acid (3 mL) and 1-octadecene (7 mL). The mixture was heated at 110 °C for 30 min to remove water and subsequently at 150 °C for 1 h before cooling to 50 °C. Then 5 mL methanol solution containing 1.6 mmol  $\text{NH}_4\text{F}$  and 1 mmol  $\text{NaOH}$  was added and the solution was stirred at 50 °C for 60 min. The solution was then heated at 110 °C under vacuum for 10 min to remove methanol and moisture, followed by heating at 300 °C for 60 min under argon atmosphere. After cooling down to room temperature, excessive amount of ethanol was poured into the solution. The resultant mixture was separated by centrifugation, washed with cyclohexane and ethanol several times, and finally redispersed in cyclohexane.

The crystal structure of the samples was analyzed by X-ray diffraction analysis (XRD, Rigaku SmartLab, Tokyo, Japan) using a  $\text{Cu K}\alpha$  radiation. Transmission electron microscopy (TEM) measurements were carried out on a Philips CM-20 transmission electron microscope (FEI, Hillsboro, OR, USA) operating at an acceleration voltage of 200 kV. Photoluminescence spectra were recorded at room temperature with an F-4600 spectrophotometer (Hitachi, Tokyo, Japan) with the excitation

source adapted to a fiber couple diode laser. All spectra were obtained at room temperature from cyclohexane dispersions of the nanoparticles (1 wt.%) at an excitation power density of  $20 \text{ W cm}^{-2}$ .

#### 4. Conclusions

In summary, we have demonstrated an alkaline earth doping approach to tuning the size and phase of  $\text{NaYF}_4$  nanoparticles following a consistent synthetic procedure.  $\text{Sr}^{2+}$  dopant ions are found to promote the formation of cubic phase  $\text{NaYF}_4$ , mainly owing to the large ionic size that resists dense atom packing in the hexagonal structure. By contrast,  $\text{Ca}^{2+}$  dopant ions with a relatively small ionic size only display weak effect on phase transformation of the  $\text{NaYF}_4$  nanoparticle. However, it allows fine-tuning of the nanoparticle size through surface charge modification. The doping approach described here represents a general strategy to expand the range of nanoparticle products that can be accessed by a particular synthetic method.

#### Acknowledgments

This study was supported by start-up grant (No. 7200317 and No. 9610257) from CityU and fundamental research grant (No. R-IND5101) from the Science Technology and Innovation Committee of Shenzhen Municipality.

#### Conflicts of Interest

The authors declare no conflict of interest.

#### References

1. Wang, F.; Wang, J.; Liu, X. Direct evidence of a surface quenching effect on size-dependent luminescence of upconversion nanoparticles. *Angew. Chem. Int. Ed.* **2010**, *49*, 7456–7460.
2. Tu, D.; Liu, Y.; Zhu, H.; Li, R.; Liu, L.; Chen, X. Breakdown of crystallographic site symmetry in lanthanide-doped  $\text{NaYF}_4$  crystals. *Angew. Chem. Int. Ed.* **2013**, *52*, 1128–1133.
3. Aebischer, A.; Hostettler, M.; Hauser, J.; Kramer, K.; Weber, T.; Gudel, H.U.; Burgi, H.B. Structural and spectroscopic characterization of active sites in a family of light-emitting sodium lanthanide tetrafluorides. *Angew. Chem. Int. Ed.* **2006**, *45*, 2802–2806.
4. Johnson, J.C.; Choi, H.J.; Knutsen, K.P.; Schaller, R.D.; Yang, P.; Saykally, R.J. Single gallium nitride nanowire lasers. *Nat. Mater.* **2002**, *1*, 106–110.
5. Li, G.; Li, C.; Zhang, C.; Cheng, Z.; Quan, Z.; Peng, C.; Lin, J.  $\text{Tm}^{3+}$  and/or  $\text{Dy}^{3+}$  doped  $\text{LaOCl}$  nanocrystalline phosphors for field emission displays. *J. Mater. Chem.* **2009**, *19*, 8936–8943.
6. Fischer, S.; Goldschmidt, J.; Loper, P.; Bauer, G.; Bruggemann, R.; Kramer, K.; Biner, D.; Hermle, M.; Glunz, S. Enhancement of silicon solar cell efficiency by upconversion: Optical and electrical characterization. *J. Appl. Phys.* **2010**, *108*, doi:10.1063/1.3478742.
7. Wang, F.; Banerjee, D.; Liu, Y.; Chen, X.; Liu, X. Upconversion nanoparticles in biological labeling, imaging, and therapy. *Analyst* **2010**, *135*, 1839–1854.

8. Liu, Y.; Chen, M.; Cao, T.; Sun, Y.; Li, C.; Liu, Q.; Yang, T.; Yao, L.; Feng, W.; Li, F. A cyanine-modified nanosystem for *in vivo* upconversion luminescence bioimaging of methylmercury. *J. Am. Chem. Soc.* **2013**, *135*, 9869–9876.
9. Haase, M.; Schafer, H. Upconverting nanoparticles. *Angew. Chem. Int. Ed.* **2011**, *50*, 5808–5829.
10. Liu, Q.; Feng, W.; Yang, T.; Yi, T.; Li, F. Upconversion luminescence imaging of cells and small animals. *Nat. Protoc.* **2013**, *8*, 2033–2044.
11. Corstjens, P.L.; Zuiderwijk, M.; Tanke, H.J.; van der Ploeg-van Schip, J.J.; Ottenhoff, T.H.; Geluk, A. A user-friendly, highly sensitive assay to detect the IFN- $\gamma$  secretion by T cells. *Clin. Biochem.* **2008**, *41*, 440–444.
12. Wang, H.-Q.; Batentschuk, M.; Osvet, A.; Pinna, L.; Brabec, C.J. Rare-earth ion doped up-conversion materials for photovoltaic applications. *Adv. Mater.* **2011**, *23*, 2675–2680.
13. Su, L.T.; Karuturi, S.K.; Luo, J.; Liu, L.; Liu, X.; Guo, J.; Sum, T.C.; Deng, R.; Fan, H.J.; Liu, X.; *et al.* Photon upconversion in hetero-nanostructured photoanodes for enhanced near-infrared light harvesting. *Adv. Mater.* **2013**, *25*, 1603–1607.
14. Huang, X.; Han, S.; Huang, W.; Liu, X. Enhancing solar cell efficiency: The search for luminescent materials as spectral converters. *Chem. Soc. Rev.* **2013**, *42*, 173–201.
15. Shalav, A.; Richards, B.S.; Trupke, T.; Krämer, K.W.; Güdel, H.U. Application of NaYF<sub>4</sub>:Er<sup>3+</sup> up-converting phosphors for enhanced near-infrared silicon solar cell response. *Appl. Phys. Lett.* **2005**, *86*, doi:10.1063/1.1844592.
16. Mai, H.-X.; Zhang, Y.-W.; Si, R.; Yan, Z.-G.; Sun, L.-D.; You, L.-P.; Yan, C.-H. High-quality sodium rare-earth fluoride nanocrystals controlled synthesis and optical properties. *J. Am. Chem. Soc.* **2006**, *128*, 6426–6436.
17. Boyer, J.-C.; Vetrone, F.; Cuccia, L.A.; Capobianco, J.A. Synthesis of colloidal upconverting NaYF<sub>4</sub> nanocrystals doped with Er<sup>3+</sup>, Yb<sup>3+</sup> and Tm<sup>3+</sup>, Yb<sup>3+</sup> via thermal decomposition of lanthanide trifluoroacetate precursors. *J. Am. Chem. Soc.* **2006**, *128*, 7444–7445.
18. Ahmad, S.; Prakash, G.V.; Nagarajan, R. Hexagonally ordered KLaF<sub>4</sub> host: Phase-controlled synthesis and luminescence studies. *Inorg. Chem.* **2012**, *51*, 12748–12754.
19. Xu, Z.; Kang, X.; Li, C.; Hou, Z.; Zhang, C.; Yang, D.; Li, G.; Lin, J. Ln<sup>3+</sup> (Ln = Eu, Dy, Sm, and Er) ion-doped YVO<sub>4</sub> nano/microcrystals with multiform morphologies: Hydrothermal synthesis, growing mechanism, and luminescent properties. *Inorg. Chem.* **2010**, *49*, 6706–6715.
20. Schäfer, H.; Ptacek, P.; Eickmeier, H.; Haase, M. Synthesis of hexagonal Yb<sup>3+</sup>, Er<sup>3+</sup>-doped NaYF<sub>4</sub> nanocrystals at low temperature. *Adv. Funct. Mater.* **2009**, *19*, 3091–3097.
21. Yi, G.S.; Chow, G.M. Synthesis of hexagonal-phase NaYF<sub>4</sub>:Yb,Er and NaYF<sub>4</sub>:Yb,Tm nanocrystals with efficient up-conversion fluorescence. *Adv. Funct. Mater.* **2006**, *16*, 2324–2329.
22. Wang, L.; Li, Y. Controlled synthesis and luminescence of lanthanide doped NaYF<sub>4</sub> nanocrystals. *Chem. Mater.* **2007**, *19*, 727–734.
23. Wang, X.; Zhuang, J.; Peng, Q.; Li, Y. A general strategy for nanocrystal synthesis. *Nature* **2005**, *437*, 121–124.
24. Wang, F.; Han, Y.; Lim, C.S.; Lu, Y.; Wang, J.; Xu, J.; Chen, H.; Zhang, C.; Hong, M.; Liu, X. Simultaneous phase and size control of upconversion nanocrystals through lanthanide doping. *Nature* **2010**, *463*, 1061–1065.

25. Zhao, C.; Kong, X.; Liu, X.; Tu, L.; Wu, F.; Zhang, Y.; Liu, K.; Zeng, Q.; Zhang, H. Li<sup>+</sup> ion doping: An approach for improving the crystallinity and upconversion emissions of NaYF<sub>4</sub>:Yb<sup>3+</sup>, Tm<sup>3+</sup> nanoparticles. *Nanoscale* **2013**, *5*, 8084–8089.
26. Lei, L.; Chen, D.; Huang, P.; Xu, J.; Zhang, R.; Wang, Y. Modifying the size and uniformity of upconversion Yb/Er:NaGdF<sub>4</sub> nanocrystals through alkaline-earth doping. *Nanoscale* **2013**, *5*, doi:10.1039/C3NR03497F.
27. Chen, D.; Huang, P.; Yu, Y.; Huang, F.; Yang, A.; Wang, Y. Dopant-induced phase transition: A new strategy of synthesizing hexagonal upconversion NaYF<sub>4</sub> at low temperature. *Chem. Commun.* **2011**, *47*, 5801–5803.
28. Chen, D.; Yu, Y.; Huang, F.; Lin, H.; Huang, P.; Yang, A.; Wang, Z.; Wang, Y. Lanthanide dopant-induced formation of uniform sub-10 nm active-core/active-shell nanocrystals with near-infrared to near-infrared dual-modal luminescence. *J. Mater. Chem.* **2012**, *22*, 2632–2640.
29. Chen, D.; Wang, Y. Impurity doping: a novel strategy for controllable synthesis of functional lanthanide nanomaterials. *Nanoscale* **2013**, *5*, 4621–4637.
30. Chen, D.; Yu, Y.; Huang, F.; Wang, Y. Phase transition from hexagonal LnF<sub>3</sub> (Ln = La, Ce, Pr) to cubic Ln<sub>0.8</sub>M<sub>0.2</sub>F<sub>2.8</sub> (M = Ca, Sr, Ba) nanocrystals with enhanced upconversion induced by alkaline-earth doping. *Chem. Commun.* **2011**, *47*, 2601–2603.
31. Cheng, Q.; Sui, J.; Cai, W. Enhanced upconversion emission in Yb<sup>3+</sup> and Er<sup>3+</sup> codoped NaGdF<sub>4</sub> nanocrystals by introducing Li<sup>+</sup> ions. *Nanoscale* **2012**, *4*, 779–784.
32. Yu, X.; Li, M.; Xie, M.; Chen, L.; Li, Y.; Wang, Q. Dopant-controlled synthesis of water-soluble hexagonal NaYF<sub>4</sub> nanorods with efficient upconversion fluorescence for multicolor bioimaging. *Nano Res.* **2010**, *3*, 51–60.
33. Wang, H.-Q.; Tilley, R.D.; Nann, T. Size and shape evolution of upconverting nanoparticles using microwave assisted synthesis. *CrystEngComm* **2010**, *12*, 1993–1996.
34. Dou, Q.; Zhang, Y. Tuning of the structure and emission spectra of upconversion nanocrystals by alkali ion doping. *Langmuir* **2011**, *27*, 13236–13241.
35. Zhang, W.H.; Wang, F.; Zhang, W.D. Phase transformation of ultrathin nanowires through lanthanide doping: From InOOH to rh-In<sub>2</sub>O<sub>3</sub>. *Dalton Trans.* **2013**, *42*, 4361–6364.
36. Feng, X.; Sayle, D.C.; Wang, Z.L.; Paras, M.S.; Santora, B.; Sutorik, A.C.; Sayle, T.X.; Yang, Y.; Ding, Y.; Wang, X.; *et al.* Converting ceria polyhedral nanoparticles into single-crystal nanospheres. *Science* **2006**, *312*, 1504–1508.
37. Zhang, F.; Wan, Y.; Yu, T.; Zhang, F.; Shi, Y.; Xie, S.; Li, Y.; Xu, L.; Tu, B.; Zhao, D. Uniform nanostructured arrays of sodium rare-earth fluorides for highly efficient multicolor upconversion luminescence. *Angew. Chem. Int. Ed.* **2007**, *46*, 7976–7979.
38. Shsannon, R.D. Revised effective ionic radii and systematic studies of interatomic distances in halides and chalcogenides. *Acta Cryst. A* **1976**, *32*, 751–767.
39. Joint Committee on Powder Diffraction Standards (JCPDS) International Centre for Diffraction Data; File Number 16-0334; JCPDS International Centre for Diffraction Data: Philadelphia, PA, USA, 2001.
40. Joint Committee on Powder Diffraction Standards (JCPDS) International Centre for Diffraction Data; File Number 06-0262; JCPDS International Centre for Diffraction Data: Philadelphia, PA, USA, 2001.

41. Joint Committee on Powder Diffraction Standards (JCPDS) International Centre for Diffraction Data; File Number 77-2042; JCPDS International Centre for Diffraction Data: Philadelphia, PA, USA, 2001.
42. Chen, D.; Yu, Y.; Huang, F.; Huang, P.; Yang, A.; Wang, Y. Modifying the size and shape of monodisperse bifunctional alkaline-earth fluoride nanocrystals through lanthanide doping. *J. Am. Chem. Soc.* **2010**, *132*, 9976–9978.

© 2013 by the authors; licensee MDPI, Basel, Switzerland. This article is an open access article distributed under the terms and conditions of the Creative Commons Attribution license (<http://creativecommons.org/licenses/by/3.0/>).